Light scattering by an array of birefringent optical waveguides: theoretical foundations

J. Limeres and M. L. Calvo

Departamento de Óptica, Universidad Complutense de Madrid, Spain

J. M. Enoch

School of Optometry, University of California, Berkeley, Berkeley, California 94720-2020

V. Lakshminarayanan

School of Optometry and Department of Physics and Astronomy, University of Missouri, Saint Louis, Missouri 63121-4499

Received July 17, 2002; revised manuscript received December 26, 2002

We develop a computational method for calculating the spatial profile of the electromagnetic field after scattering by an array of waveguides. Our formalism is very general and includes chromatic dependence, the influence of the array arrangement, and other effects such as the effect of stress. Our calculations of the amplitude and phase of scattered light provide valuable information about the features of the waveguides. These results can be applied to different areas of study, such as biological waveguides and fiber sensing. © 2003 Optical Society of America

OCIS codes: 060.2310, 060.2370, 060.4370, 230.7370, 290.4210, 330.5310.

1. INTRODUCTION

Scattering of light by a bundle of anisotropic optical fibers (waveguides) is an interesting tool with which to obtain information on the geometrical—i.e., arrangement or size—and optical properties of the array of fibers. In connection with the formulation of light scattering by single isotropic optical waveguides, there are a number of well-developed methods in the literature,[1,2] and such useful approximations as the well-established eikonal are commonly applied.[3] On the other hand, multiple scattering has been treated within several theoretical frameworks. It is especially worth mentioning the analysis of light scattering by an array of N fixed isotropic obstacles with arbitrary shape, which has been treated by considering the formalism of multiple scattering as an application of quantum-mechanical multiple scattering in the context of classical fields.[4] Also, multiple scattering by volume gratings has been solved through a modified Fujiwara's theory.[5] However, to our knowledge, none of these formalisms have yet been applied to study multiple scattering by an array of N isotropic optical waveguides. Moreover, scattering by multiple anisotropic waveguides, which is the subject of this work, has scarcely been considered. This can be attributed to the mathematical complications that arise as a result of the tensor formalism that is required for including the anisotropy of the medium. In an earlier work, we have treated multiple scattering by an array of N birefringent optical waveguides with cylindrical symmetry.[6] We have shown that the solution in the form of a system of two coupled integral equations is rather complex to be applied in numerical calculations, even for the simplest case of two waveguides.

In this paper, we present a numerical procedure to calculate scattering by multiple, anisotropic, cylindrical waveguides that has its basis in a first-order approximation for multiple scattering. Our general formalism allows us to consider different geometrical arrangements for packing and to analyze the influence of geometrical and optical parameters on the amplitude and phase of the total scattered light field. In particular, arrays of fibers with various wavelength sensitivities can be considered, thus allowing us to simulate a polychromatic response. Finally, other properties that affect the scattering process, such as photoelasticity, can also be included. Such fibers are of current practical interest. For example, applications of our method include simulation of retinal photoreceptors and biological waveguides, polarimetric fiber-optic sensors, and, in general, mechanical stress sensors. It should be remarked that multiple-scattering theories have been previously used within the context of ocular structures.[7,8] These works, however, were not related to photoreceptor optics, but to different scattering phenomena, such as the propagation of light through the cornea[7] or multiple scattering by cellular organelles at the retinal nerve fiber layer.[8] An important distinction of these formalisms is that our model, being more general, allows us to take into account the waveguiding properties that characterize the behavior of retinal photoreceptors. With regard to optical-fiber-based sensors, we point out here that previous work presented by other authors requires a modal analysis and far-field-radiation-pattern character-

0740-3224/2003/071542-08$15.00

ization for particular modal orders.[9] Our method, with its basis in the analysis of the forward-scattering intensity pattern, would require a less sophisticated and therefore less costly procedure.

The paper is organized as follows. We introduce the conditions of our physical system in Section 2. In Section 3 we review the mathematical formulation of light scattering for a single anisotropic waveguide. Then we discuss the approaches that have allowed us to reach a simple matrix equation that can be numerically integrable. Section 4 describes in detail the numerical procedure. In Section 5, the theoretical formalism is generalized for an array of waveguides by way of the sampling theory. In Section 6, we incorporate photoelasticity into the model. This mechano-optical effect consists in a change in birefringence induced by mechanical strain. Section 7 contains some numerical results and applications. Finally, in Section 8, we summarize and draw the main conclusions of our work.

2. PHYSICAL CONDITIONS

We consider N parallel, infinite, dielectric cylindrical waveguides along the Z axis inside an infinite optical medium having refractive index n_O. As incident light is interacting with the fiber package, a multiple-scattering phenomenon takes place. Analysis of the complex amplitude distribution associated with the scattered field will provide information on the optical properties of the fiber package (see Fig. 1).

Let the two-dimensional vector $\boldsymbol{\rho} \equiv (x, y)$ denote a generic position in the XY plane and let d be the average distance between adjacent waveguides. Consider a general case of birefringent, optically active waveguides. We need to introduce the tensor representing the dielectric permittivity associated with these media. For the single isolated ith fiber

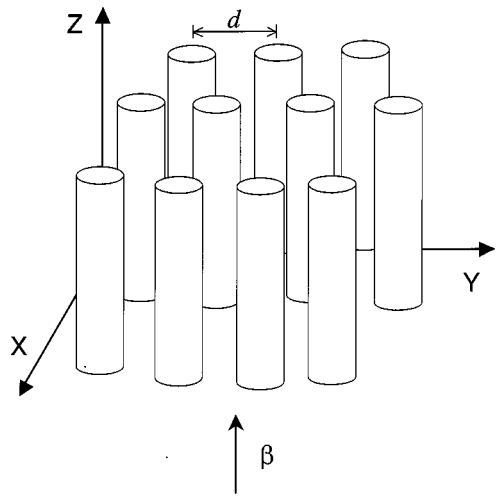

Fig. 1. N coupled waveguides; configuration for each single fiber as in Fig. 2. $d \equiv$ average distance between two adjacent (parallel) fibers. The impact plane XY defines the plane where the amplitude of the light scattered by the fiber array is determined (see text for details).

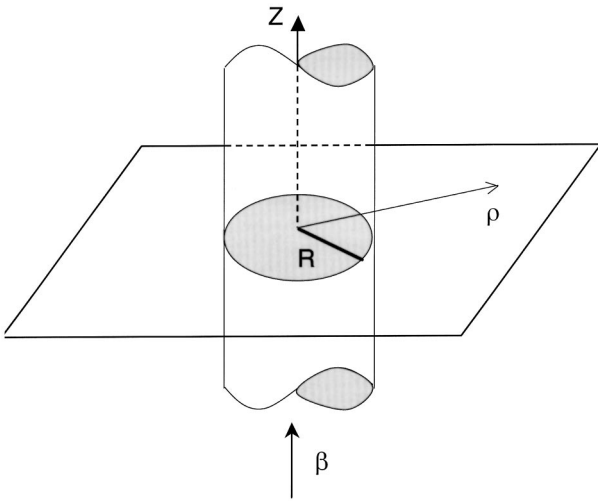

Fig. 2. Model of an individual fiber; the wave vector of the incoming radiation $\boldsymbol{\beta}$ is defined at the Z direction (parallel to the optic axis of the waveguide). According to the properties of birefringent media, the electric displacement vector is defined at the XY plane. The magnetic field is plane-polarized at the XY plane. In assuming this model, the propagation modes are considered with propagation constant β, along with the light scattering. This is the configuration considered in the present model [see Eqs. (2) and (3)].

$$\varepsilon(\mathbf{p}) = \begin{bmatrix} \varepsilon_{11} & \varepsilon_{12} & 0 \\ \varepsilon_{21} & \varepsilon_{22} & 0 \\ 0 & 0 & \varepsilon_{33} \end{bmatrix}. \tag{1}$$

In Eq. (1), $\varepsilon(\boldsymbol{\rho})$ is the dielectric permittivity tensor inside the ith fiber. In general, it will be a function of the two-dimensional vector $\boldsymbol{\rho}$. The cross-sectional area of the ith fiber is $\Omega_i = \pi R_i^2$, R_i being the radius of the ith fiber. If the medium is not optically active, then $\varepsilon_{12} = \varepsilon_{21} = 0$. For the case of an isotropic fiber all the elements of the diagonal of the tensor have the same value $\varepsilon_{ii} = \varepsilon$.

Let us assume that an incident, monochromatic, plane-polarized scalar wave interacts with the ith fiber. We shall assume that the magnetic field $\mathbf{h} = (\mathbf{h}_x, \mathbf{h}_y, 0)$ is plane polarized at the XY plane (see Fig. 2). The wave vector $\boldsymbol{\beta}$ of the incoming radiation is defined along the Z direction (parallel to the optic axis of the waveguide). The magnetic scalar field $\mathbf{h}_{\text{in}}(\boldsymbol{\rho})$ associated with the incoming wave is

$$\mathbf{h}_{\text{in}}(\boldsymbol{\rho}) = \mathbf{h}_0(\boldsymbol{\rho})\exp(i\beta z). \tag{2}$$

$\mathbf{h}_{\text{in}}(\boldsymbol{\rho})$ is transverse to the Z axis as displayed in Fig. 2(a). In Eq. (2), β is the modulus of the wave-vector propagation associated with the incoming wave, defined above. For convenience we shall analyze the magnetic scattered field in the remainder of this paper.

3. LIGHT SCATTERING BY A BIREFRINGENT OPTICAL WAVEGUIDE

Before introducing the mathematical formalism, we have to consider some required mathematical properties of the behavior of the scattered-amplitude function. This function and its first derivatives are continuous inside Ω_i, al-

though they may be discontinuous across the external boundary of the ith waveguide, which, for simplicity, we assume to be unclad.

The boundary conditions for a dielectric interface are the usual ones.[10] After the interaction of the incoming field with the ith fiber, the total transverse magnetic field arising from the fiber is

$$\mathbf{h}_{\mathrm{scatt}}(\boldsymbol{\rho}) = \mathbf{h}_i(\boldsymbol{\rho})\exp(i\beta z). \tag{3}$$

When we start from Maxwell's equations and use standard Green's function techniques, some direct (although lengthy) calculations yield[11]

$$\mathbf{h}_i(\boldsymbol{\rho}) = \mathbf{h}^{(0)}(\boldsymbol{\rho}) + \int_{\Omega_i} \mathrm{d}^2\boldsymbol{\rho}'[(1/4i)H_0^{(1)}(K|\boldsymbol{\rho}-\boldsymbol{\rho}'|)\hat{P}_1(\boldsymbol{\rho}') + \hat{P}_2(\boldsymbol{\rho},\boldsymbol{\rho}')]\mathbf{h}_i(\boldsymbol{\rho}'), \tag{4}$$

where $K^2 = (n_0 2\pi/\lambda)^2 - \beta^2$, $\lambda \equiv$wavelength of light, $n_0 \equiv$refractive index of the medium, and $H_0^{(1)} \equiv$Hankel function of the first kind and zeroth order. In this equation, $\int_{\Omega i}\mathrm{d}^2\boldsymbol{\rho}$ denotes the integral over the total cross section Ω_i of the ith waveguide. Finally, matrices $\hat{\mathbf{P}}_1$ and $\hat{\mathbf{P}}_2$ are given by

$$\hat{\mathbf{P}}_1(\boldsymbol{\rho}') = -K^2\begin{bmatrix} \varepsilon_{22}-1 & 0 \\ 0 & \varepsilon_{11}-1 \end{bmatrix}, \tag{5a}$$

$$\hat{\mathbf{P}}_2(\boldsymbol{\rho},\boldsymbol{\rho}') = \frac{1}{4i\varepsilon_{33}}\begin{bmatrix} -(\varepsilon_{22}-\varepsilon_{33})\dfrac{\partial^2 H_0^{(1)}(K|\boldsymbol{\rho}-\boldsymbol{\rho}'|)}{\partial x'^2} & (\varepsilon_{22}-\varepsilon_{33})\dfrac{\partial^2 H_0^{(1)}(K|\boldsymbol{\rho}-\boldsymbol{\rho}'|)}{\partial x'\partial y'} \\ -(\varepsilon_{33}-\varepsilon_{11})\dfrac{\partial^2 H_0^{(1)}(K|\boldsymbol{\rho}-\boldsymbol{\rho}'|)}{\partial y'\partial x'} & (\varepsilon_{33}-\varepsilon_{11})\dfrac{\partial^2 H_0^{(1)}(K|\boldsymbol{\rho}-\boldsymbol{\rho}'|)}{\partial y'^2} \end{bmatrix}. \tag{5b}$$

The circumflex symbol ˆ is used throughout to designate matrices. In this expression $\boldsymbol{\rho}' \equiv (x', y')$.

Note that the first term on the right-hand side of Eq. (4) is just the amplitude of the incident plane wave. The second contribution contains information about the scattering process. It depends on the scatterer's features (size relative to the light wavelength λ, geometry, material parameters, etc.) through the matrices $\hat{\mathbf{P}}_1$ and $\hat{\mathbf{P}}_2$.

The integral Eq. (4) can be formally solved by indefinite iteration. However, for weak scattering processes, it is acceptable to keep only the first term of the iteration. Such approach leads to the following formula:

$$\mathbf{h}_i(\boldsymbol{\rho}) = \mathbf{h}^{(0)}(\boldsymbol{\rho}) + \int_{\Omega_i}\mathrm{d}^2\boldsymbol{\rho}'\left[\frac{1}{4i}H_0^{(1)}(K|\boldsymbol{\rho}-\boldsymbol{\rho}'|)\hat{\mathbf{P}}_1(\boldsymbol{\rho}') + \hat{\mathbf{P}}_2(\boldsymbol{\rho},\boldsymbol{\rho}')\right]\mathbf{h}^{(0)}(\boldsymbol{\rho}). \tag{6}$$

Before developing our mathematical approach, we will introduce a few simplifications. First, let us consider a homogeneous fiber, that is, $\varepsilon \neq \varepsilon(\boldsymbol{\rho})$. Second, we assume that the symmetry properties of the birefringent waveguide correspond to those of a uniaxial crystal.[12] Consequently, we have $\varepsilon_{12} = \varepsilon_{21} = 0$ and $\varepsilon_{11} = \varepsilon_{22}$. After these assumptions, expressions for $\hat{\mathbf{P}}_1$ and $\hat{\mathbf{P}}_2$ can be substantially simplified:

$$\hat{\mathbf{P}}_1 = -K^2\begin{bmatrix} \varepsilon_{11}-1 & 0 \\ 0 & \varepsilon_{11}-1 \end{bmatrix}, \tag{7a}$$

$$\hat{\mathbf{P}}_2(\boldsymbol{\rho},\boldsymbol{\rho}') = \frac{1}{4i\varepsilon_{33}}(\varepsilon_{33}-\varepsilon_{11})\begin{bmatrix} \dfrac{\partial^2 H_0^{(1)}}{\partial x'^2} & -\dfrac{\partial^2 H_0^{(1)}}{\partial x'\partial y'} \\ -\dfrac{\partial^2 H_0^{(1)}}{\partial y'\partial x'} & \dfrac{\partial^2 H_0^{(1)}}{\partial y'^2} \end{bmatrix}. \tag{7b}$$

Finally, we will assume that the incident plane wave has constant amplitude $\mathbf{h}^{(0)}(\boldsymbol{\rho}) = \mathbf{h}^{(0)}$. In this situation, the final result for the scattering amplitude of the magnetic field can be written symbolically as

$$\mathbf{h}_i(\boldsymbol{\rho}) = \mathbf{h}^{(0)} - \frac{1}{4i}\hat{\mathbf{P}}_1 I_1 h^{(0)} + \hat{\mathbf{P}}_2\hat{\mathbf{I}}_2\mathbf{h}^{(0)}, \tag{8}$$

where I_1 denotes the integral of the Hankel function $H_0^{(1)}$ within the cross section Ω_i of the cylindrical waveguide (see Fig. 1):

$$I_1 = \int_{\Omega}\mathrm{d}^2\boldsymbol{\rho}' H_0^{(1)}(K|\boldsymbol{\rho}-\boldsymbol{\rho}'|), \tag{9}$$

and matrix $\hat{\mathbf{I}}_2$ is written as

$$\hat{\mathbf{I}}_2 = \frac{1}{4i\varepsilon_{33}}(\varepsilon_{33}-\varepsilon_{11})\begin{bmatrix} \mathbf{I}_2^{xx} & -\mathbf{I}_2^{xy} \\ -\mathbf{I}_2^{yx} & \mathbf{I}_2^{yy} \end{bmatrix}. \tag{10}$$

The elements $\mathbf{I}_2^{\alpha,\beta}(\alpha = x, y)$ of matrix $\hat{\mathbf{I}}_2$ correspond to integration of the second derivatives of $H_0^{(1)}$ within the area Ω_i, that is,

$$\mathbf{I}_2^{\alpha\beta} = \int_{\Omega}\mathrm{d}^2\boldsymbol{\rho}'\frac{\partial^2 H_0^{(1)}}{\partial x_\alpha \partial x_\beta}(K|\boldsymbol{\rho}-\boldsymbol{\rho}'|). \tag{11}$$

Note that in Eqs. (5)–(9), the symbol $\boldsymbol{\rho}$ denotes a generic point in the whole XY plane, while points labeled $\boldsymbol{\rho}'$ are constrained to the area Ω_i within the fiber [see Fig. 3(a)].

Now, the problem of solving the light scattering by an optical fiber reduces to the numerical evaluation of integrals I_1 and $\mathbf{I}_2^{\alpha\beta}$.

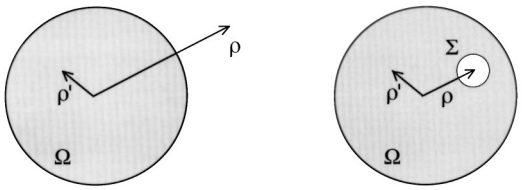

(a) (b)

Fig. 3. Integration region: (a) Circular section of a single fiber $\Omega = \pi R^2$, where R is the radius of the fiber, $\boldsymbol{\rho}$ is the point of observation, and $\boldsymbol{\rho}'$ is the radial variable of integration. In this case, $|\boldsymbol{\rho}| > R$, so $|\boldsymbol{\rho} - \boldsymbol{\rho}'| > 0$. (b) In this case, $|\boldsymbol{\rho}| < R$. Then, at $|\boldsymbol{\rho} - \boldsymbol{\rho}'| = 0$ the integrand shows a singularity; see text for details.

4. NUMERICAL PROCEDURE

Let us examine integral I_1. It can be shown that the Hankel function $H_0^{(1)}$ is integrable in the whole plane,[6] even though it diverges at the origin, that is, at $\boldsymbol{\rho} = \boldsymbol{\rho}'$. Nevertheless, to perform the numerical integration, this singularity must be carefully handled.

When calculating I_1 at a given point $\boldsymbol{\rho}$ two situations can take place:

1. If point $\boldsymbol{\rho}$ lies outside the integration area, i.e., $\boldsymbol{\rho} \notin \Omega_i$ [see Fig. 3(a)], the eventuality that $\boldsymbol{\rho} = \boldsymbol{\rho}'$ never occurs. In that case, the numerical integration can be performed straightforwardly by standard numerical methods. In particular, we used a library routine for integrating by Gaussian quadratures.[13]
2. If point $\boldsymbol{\rho}$ belongs to Ω_i [see Fig. 3(b)], we will have to deal with a locally divergent integrand. In this work we have proceeded in the following way. We define a small circular area Σ of radius $\delta \ll 1/K$ centered at $\boldsymbol{\rho}$ as shown in Fig. 3(b). Then we divide the integration space into two parts: outside and inside the area Σ. In the region outside Σ, no singularity is found, so the above-mentioned standard routine can be applied. Conversely, inside Σ the Hankel function $H_0^{(1)}$ is singular. However, since we have defined $\delta \ll 1/K$, it is permissible to replace the function $H_0^{(1)}$ by its small-argument approximation,[14] which is analytically integrable. In this way we obtain two numerical values, one corresponding to the area outside Σ, the other corresponding to the small area Σ. Finally, we sum both contributions to obtain the final result for I_1.

Evaluation of $\mathbf{I}_2^{\alpha\beta}$ is performed through a completely analogous procedure. However, additional steps are involved because the second derivatives of $H_0^{(1)}$ must also be computed. This results in a substantial increase in the computing time. Calculation of I_1 at a given spatial point takes less than 0.002 s, while the computing time of $\mathbf{I}_2^{\alpha,\beta}$ is ~1 s. The number of spatial points required to plot the surface of the scattering amplitude will determine the total computing time.

Fortunately, the scattered amplitude $\mathbf{h}_{\text{scatt}}$ is mainly dominated by the second (right-hand side) term in Eq. (8). The third contribution (right-hand side) represents a minor correction and we will neglect it in the remainder of this paper. The validity of this approximation will be discussed in Subsection 7.A. This simplification will allow us to save a large amount of computing time. For instance, to obtain a plot of 6400 spatial points (such as those shown in Figs. 6 and 7) typically requires ~15 seconds of computing time. The same calculation takes 1.5 hours if the third (right-hand side) term of Eq. (8) is included.

5. GENERALIZATION: LIGHT SCATTERING BY AN ARRAY OF BIREFRINGENT WAVEGUIDES

Let us consider now an array of parallel, cylindrical waveguides; see Fig. 1. To generalize, the single-fiber results obtained above to a bundle of N fibers, we will apply the sampling theory. Sampling methods have been used successfully to solve different optical problems.[15] In particular, a regular array of identical fibers is a very suitable candidate for treatment by the sampling approach, as has been shown in previous work on biological waveguides.[16]

In the present work we are dealing with a function with cylindrical symmetry. Hence, the sampling theorem leads to the following expression for the total field amplitude $\mathbf{h}_{\text{tot}}$:[17]

$$\mathbf{h}_{\text{tot}} = \frac{\pi}{4} \sum_m \sum_n \mathbf{h}_i(nd/2, md/2) \times \frac{J_1\{2\pi/d[(x - nd/2)^2 + (y - md/2)^2]^{1/2}\}}{2\pi/d[(x - nd/2)^2 + (y - md/2)^2]^{1/2}}, \tag{12}$$

where $\mathbf{h}_i$ is the scattered amplitude of each single fiber and J_1 is the first-order Bessel function. The summation indices n and m label the sampling points $x_n = nd/2$, $y_m = md/2$, d being the separation between adjacent fibers. Depending on the symmetry of the problem, different sampling lattices may be used. Figure 4 shows two different geometries: a Cartesian grid of nine points [Fig. 4(b)] and a radially symmetric web of seven points [Fig. 4(a)]. Both packing arrangements have been typically considered in the literature. In particular, the hexagonal lattice [Fig. 4(a)] describes the observed arrangement of photoreceptors in the human retina.[18]

Obviously, the shape of the total field must depend on the chosen lattice. In particular, the effective aperture of the array coincides with the contour of the packing.

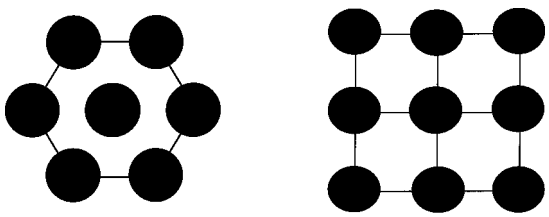

(a) (b)

Fig. 4. Packing arrangements: (a) The section of the array fits a hexagon formed by seven waveguides. (b) The section of the array fits a square formed by nine waveguides.

6. MECHANO-OPTICAL EFFECTS IN ANISOTROPIC WAVEGUIDES

It is well known that the optical properties of a dielectric waveguide can be altered by the action of external forces. The major consequence is the production of an elastic deformation affecting the birefringent properties of the medium (while maintaining the mass density). Such a phenomenon can be observed and evaluated by the photoelastic effect.[19]

For a mathematical description of this phenomenon, one needs to consider a new dielectric permittivity tensor $\tilde{\varepsilon}$ in which additional terms accounting for the photoelasticity are included. These terms are proportional to the magnitude of the external force. They correspond to the components of the so-called deformation tensor. To simplify the model we assume that the optical activity is negligible. The representation of the modified dielectric permittivity tensor is[20]

$$\tilde{\varepsilon} = \varepsilon_e \delta_{ik} + a_1 u_{ik} + a_2 u_{ll} \delta_{ik}, \tag{13}$$

where $i, k, l = 1, 2, 3$. Also, in Eq. (13) $\varepsilon_e = n_e^2$, where n_e is the refractive index of the extraordinary ray. In our case (Fig. 1) and assuming a uniaxial medium $n_e = \sqrt{\varepsilon_{33}/\varepsilon_0}$, where ε_0 is the dielectric permittivity associated with vacuum, δ_{ik} is the Kronecker delta, a_i are the so-called elastic-optical constants of the medium, and u_{ik} are the components of the stress tensor. The latter are proportional to the transverse force per unit length applied to each waveguide. Let us assume that the force is applied in the Y direction (see Fig. 5); the mechanical effects will be produced in the XY plane, and we define

$$u_{11} = \frac{|\mathbf{F}|}{\pi R_i^2},$$
$$u_{22} = -3u_{11}, \tag{14}$$
$$u_{33} = 0.$$

Also, we consider that under the external force, each waveguide behaves as a uniaxial crystal. Under this assumption the dielectric permittivity tensor reads

$$\tilde{\varepsilon} = \begin{bmatrix} \tilde{\varepsilon}_{11} & 0 & 0 \\ 0 & \tilde{\varepsilon}_{22} & 0 \\ 0 & 0 & \tilde{\varepsilon}_{33} \end{bmatrix}, \tag{15}$$

where

$$\tilde{\varepsilon}_{11} = \varepsilon_e + a_1 u_{11} + a_2 u_{22} + a_2 u_{33},$$
$$\tilde{\varepsilon}_{22} = \varepsilon_e + a_2 u_{11} + a_1 u_{22} + a_2 u_{33},$$
$$\tilde{\varepsilon}_{33} = \varepsilon_e + a_1 u_{11} + a_2 u_{22} + a_1 u_{33}. \tag{16}$$

If we use Eq. (16) in Eqs. (7a) and (7b) and introduce these expressions into Eq. (8), we obtain the scattering amplitude associated with a birefringent fiber having photoelastic properties. Equations (15) and (16) are the key to the subsequent numerical estimates.

The extension to the multiple-scattering formulation is similar to Eq. (12), the only condition being that now one has to use Eqs. (15) and (16) for the dielectric permittivity tensor instead of Eq. (1).

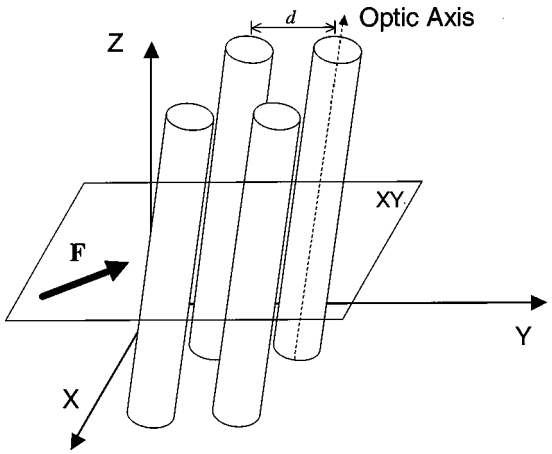

Fig. 5. A model for mechano-optical effect. A weak external force **F** is applied and defined in some arbitrary XY plane. The conditions of incidence of light are similar to those of Figs. 1 and 2. Note that here the optic axis may have a certain arbitrary angle with respect to the Z axis (original optic axis prior to force application).

7. NUMERICAL APPLICATIONS

A. Intensity and Phase Distribution of Light Scattered by a Single Fiber

We have applied our computational method to investigate light scattering by a birefringent, cylindrical waveguide with ordinary refractive index $n_o = 1.34$ and extraordinary refractive index $n_e = 1.35$. By numerically solving Eq. (8) we have been able to obtain the intensity and phase of the scattered light. We must recall here that we have neglected the third (right-hand side) term of Eq. (8). The validity of this approximation will be discussed at the end of this subsection. Note that the remaining term of Eq. (8) is a diagonal matrix. This means that, in this approach, the scattering process does not lead to any coupling between the two orthogonal components of the field X and Y. Then each component can be treated separately, and consequently the vectorial problem of scattering of a planar, linearly polarized wave can be reduced to the simpler problem of two independent scalar calculations, one corresponding to each component. Moreover, both components are given by completely analogous formulas. Therefore, we need only analyze the behavior of one of them, since the result is immediately applicable to the other.

The three panels of Fig. 6 illustrate the spatial dependence of the scattering intensity $|h_{\text{scatt}}|^2$. A three-dimensional plot has been drawn to show simultaneously the dependence on X and Y. Hence, it is easily noted that, as a result of the cylindrical symmetry of the physical problem, the spatial profile exhibits radial symmetry. In this figure we show the influence of the radius of the optical fiber for a fixed wavelength, $\lambda = 500$ nm. We have considered in Figs. 6(a)–6(c) three values of the fiber's radius R: 6(a) $R = 0.5\ \mu$m, 6(b) $R = 0.75\ \mu$m, and 6(c) $R = 1.5\ \mu$m. Note that the scattering peak, centered at the origin, broadens as the radius R decreases for a fixed wavelength, as expected.

A typical plot of the phase of the scattered field is shown in Fig. 7. The phase exhibits a minimum value of $\sim\pi/4$ rad at the center of the fiber ($r = 0$) and increases monotonically as we move away from the origin. It shows an increase of nearly $\pi/4$ rad as ρ goes from 0 to $\sim R$. For $r \tau R$, the phase exhibits a growing quasi-linear behavior. As before, the wavelength $\lambda = 500$ nm has been considered.

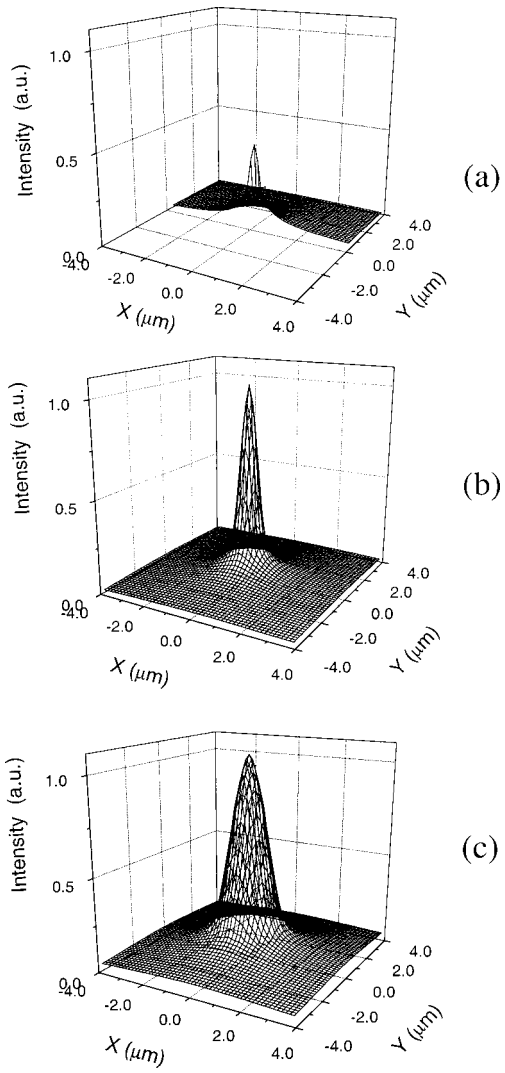

Fig. 6. Numerical analysis of Eq. (6) for the profile of the total field scattered by a single waveguide. The intensity of the scattered light is a function of the position. We consider three values for the ratio of the fiber radius to the wavelength of the incoming radiation: (a) $R/\lambda = 0.67$, (b) $R/\lambda = 1.33$, and (c) $R/\lambda = 2.67$.

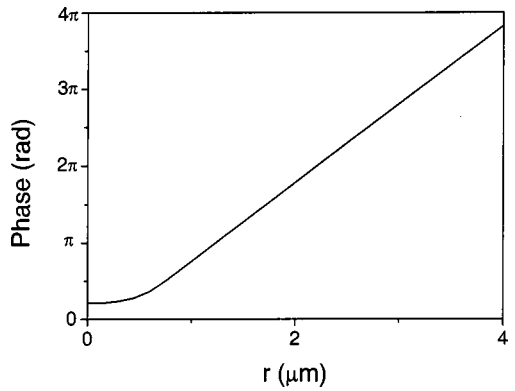

Fig. 7. Representation of the phase of the complex scattering-field amplitude as a function of the spatial coordinates X and Y.

To finish this subsection, let us evaluate the magnitude of the third (right-hand side) contribution to the scattered field in Eq. (8), which we have previously neglected in these results. The neglected term depends on (1) the value of the integrals of the second derivatives of $\mathbf{I}_2^{\alpha\beta}$, and (2) the birefringence. The values of all four integrals $\mathbf{I}_2^{\alpha\beta}$ are 2.5 to 10 times smaller than for I_1; that is $\mathbf{I}_2^{\alpha\beta}/\mathbf{I}_1 = 0.4$. Hence, the relative importance of the product $\hat{\mathbf{P}}_2\mathbf{I}_2$ depends on the degree of birefringence of the fiber through the factor $|\varepsilon_{33} - \varepsilon_{ii}|/\varepsilon_{33}$. In our calculations, we have taken $\varepsilon_{33} = 1.35$ and $\varepsilon_{11} = \varepsilon_{22} = 1.34$, which leads to a value $|\varepsilon_{33} - \varepsilon_{ii}|\varepsilon_{33} < 0.01$.

B. Intensity Distribution of the Light Scattered by an Array of Fibers

In this section we will consider an array of N identical birefringent waveguides of radius $R = 0.75\ \mu$m and with the same optical properties considered in Subsection 7.A, i.e., $n_o = 1.34$ and $n_e = 1.35$. The separation between the axis of adjacent fibers is $d = 2.0\ \mu$m.

We have applied our previous results to calculate the individual contributions associated with each single fiber, i.e., the terms h_i in Eq. (12). The total scattered field h_{tot} is obtained through summation in n and m. From the computational point of view, Eq. (12) implies the calculation of the single-fiber amplitude $n \times m$ times—one for each term of the summation of Eq. (12)— at every spatial point (x, y) to be plotted. Then the number of fibers of the bundle and the number of spatial sampling points will determine the computation time. For instance, a 6400-point plot of the light field scattered by seven waveguides takes $\sim$1.5 min. In the case of $\sim$50 waveguides, the computation time would increase to $<$10 min.

We have observed that—in comparison with the case of a single fiber—the scattering by an array shows a broader peak intensity profile. We have investigated the two geometrical arrangements shown in Figs. 4(a) and (b). The scattered amplitude h_{tot} calculated for a hexagonal lattice with seven fibers is shown in Fig. 8(a); the case of a square lattice of nine fibers is presented in Fig. 8(b). Note that the shape of the spatial amplitude is slightly affected by the geometrical arrangement. In particular, the peak at the origin is narrower in the case of a square lattice, but also, secondary peaks appear that are absent in the hexagonal arrangement.

C. Effect of a Small External Force Applied to the Array of Fibers

Finally, we have investigated the effect of the external stress induced by an applied force; see Fig. 5. Without loss of generality, we have chosen our coordinate system so that the force is applied along the Y axis. Application of a force along a certain direction within the XY plane breaks the radial symmetry of the physical system. Hence, X and Y directions are no longer optically equivalent. The major effect of stress on the scattered-intensity profile is found in the value of the central peak which cor-

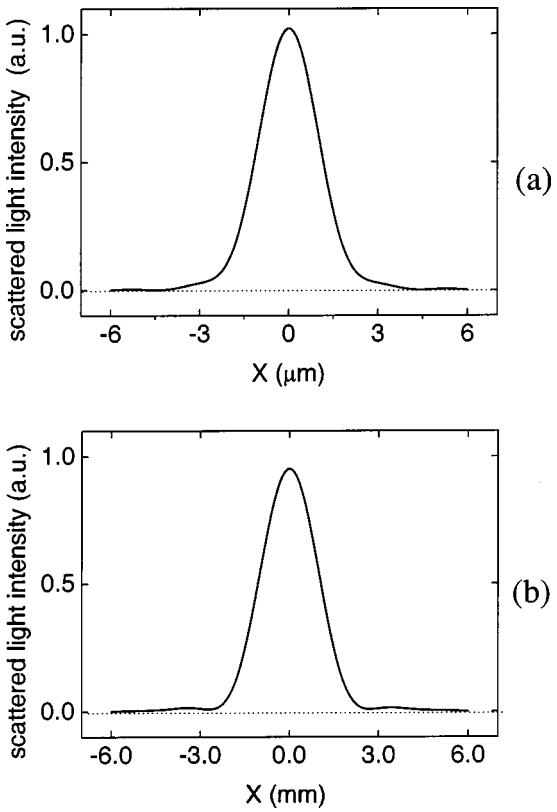

Fig. 8. Representation of the total intensity of the scattered light for different arrangements of the fibers forming the bunch (see Fig. 4): (a) seven fibers in a hexagonal lattice packing, (b) nine fibers arranged in a square lattice.

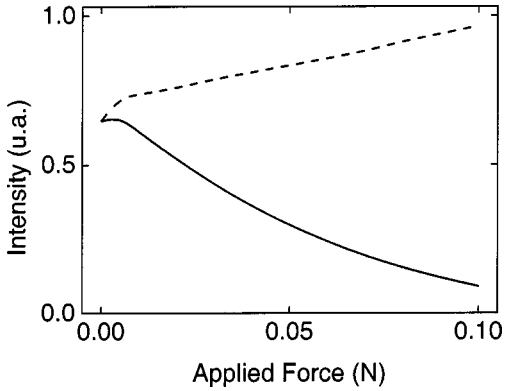

Fig. 9. Forward-scattering intensity versus the strength of the applied force. The solid curve corresponds to *X*-polarized light, the dashed curve to *Y*-polarized light.

responds to forward scattering. This is especially convenient for possible applications, since the forward direction is most suitable for scattering observation.

Our results are illustrated in Fig. 9, where the forward-scattering light intensity is plotted as a function of the strength of the applied force. The solid curve corresponds to *X*-polarized light and the dashed curve to *Y*-polarized light. The force has been varied in the range 0–0.1 N. Note that, since the force produces elastic deformation of the waveguides, an anisotropy is induced that leads to a significant difference between the response of both polarizations. For instance, for an applied force $F = 0.05$ N, a difference between them of more than 60% can be observed.

This effect has interesting possibilities for applications. First, our formalism could be the foundation of a new model for the behavior of retinal photoreceptors. In particular, it might be applied to account for quite recent experimental results[21] that revealed strains causing orderly alterations in photoreceptor orientations in observers with high myopia. Also, the authors have proposed to exploit the sensitivity of this effect, as it could be the basis for an in-fiber stress-sensing technique.[22]

8. SUMMARY AND CONCLUSIONS

We have developed a numerical model that has allowed us to solve light scattering by multiple, birefringent optical waveguides for the first time in the literature, to our knowledge. First, we have obtained the intensity of light scattered by a single waveguide by introducing some simplifying hypotheses to reduce the mathematical complexity of the problem. In addition, we have been forced to perform a two-step numerical integration to avoid singularities of the integrand. Then we have extended the single-fiber result to an array of N birefringent cylindrical waveguides by way of the sampling theory. In addition, we have considered the effect of mechanical stress by taking into account photoelasticity.

Our method allows us to calculate the intensity and phase of the scattered field. The influence of different parameters can be evaluated, which can then be used to obtain valuable information about fiber properties. For instance, we have observed a broadening of the central peak of the intensity profile as the fiber radius decreases.

With regard to optical fiber applications, the use of arrays instead of single fibers is advantageous because the former produce stronger signals more easily detectable. Moreover, biological waveguides, such us retinal photoreceptors, are found in arrays. Then we have investigated the influence of different packing arrangements of the fibers. We have found that, for a moderate size of fiber bundles ($N < 10$), different patterns lead to slight differences among the spatial profiles of the scattered light.

Finally, we have found that application of an external force breaks the radial symmetry of the physical system. This leads to a relevant difference between light polarized along or perpendicular to the direction of the applied force. This effect could be profitably used in stress-sensing procedures as an alternative to the well-known method based on modal analysis of the far-field-radiation-intensity pattern.

In conclusion, we have developed a powerful numerical tool to investigate light scattering that may be used in different applications such as characterization of birefringent optical waveguides and stress sensing. Also, our model can be applied to model the behavior of biological waveguides. Further work is currently in progress.

ACKNOWLEDGMENTS

The authors gratefully acknowledge financial support from the New Del Amo Foundation under the New Del Amo Joint Academic Project (University of California–

Universidad de Madrid) and from the Universidad Complutense de Madrid under Multidisciplinary Project PR486/97-7477/97. Partial results were presented at the 19th Congress, "Optics for the quality of life," International Commission for Optics, Florence, Italy, August 25–30, 2002.

M. L. Calvo may be reached by e-mail at mlcalvo @fis.ucm.es.

REFERENCES

1. A. W. Snyder, "Excitation and scattering of modes on a dielectric of optical fiber," IEEE Trans. Microwave Theory Tech. **MIT-17**, 1138–1144 (1969).
2. R. F. Álvarez-Estrada and M. L. Calvo, "Electromagnetic scattering by an infinite inhomogeneous dielectric cylinder: new Green's function and integral equations," J. Math. Phys. **21**, 389–394 (1980).
3. S. K. Sharma and D. J. Somerford, "Scattering of light in the Eikonal approximation," in *Progress in Optics, Vol. XXXIX*, E. Wolf, ed. (Elsevier, North-Holland, Amsterdam, 1992), Chap. III.
4. M. L. Calvo and A. Durán, "Freedholm's method for multiple scattering of electromagnetic waves by fixed obstacles," Il Nuovo Cimento **45B**, 68–76 (1978).
5. P. Cheben and M. L. Calvo, "Multiple scattering of classical electromagnetic waves by volume gratings: completion of Fujiwara's solution," J. Mod. Opt. **46**, 181–198 (1999).
6. M. L. Calvo and R. F. Álvarez-Estrada, "Coupling of dielectric waveguides," in *Max Born Centenary Conference*, M. J. Colles and D. Swift, eds., Proc. SPIE **369**, 401–406 (1982).
7. T. B. Smith, "Multiple scattering in the cornea," J. Mod. Opt. **35**, 93–101 (1988).
8. Q. Zhou and R. W. Knighton, "Light scattering and form birefringence of parallel cylindrical arrays that represent cellular organelles of the retinal nerve fiber layer," Appl. Opt. **36**, 2273–2285 (1997).
9. T. R. Wolinski, "Polarimetric optical fibers and sensors," in *Progress in Optics, Vol. XL*, E. Wolf, ed. (Elsevier, Amsterdam, 2000), Chap. I.
10. A. Snyder and J. D. Love, *Optical Waveguide Theory*, (Chapman & Hall, London, 1983), Chap. 30.
11. R. F. Alvarez-Estrada and M. L. Calvo, "Single-mode anisotropic cylindrical dielectric waveguides," Opt. Acta **30**, 481–503 (1983).
12. A. M. Benoit, K. Naoun, V. Louis-Dorr, L. Mala, and A. Raspiller, "Linear dichroism of the retinal nerve fiber layer expressed with Mueller matrices," Appl. Opt. **40**, 565–569 (2001).
13. W. H. Press, B. P. Flannery, S. A. Teukolsky, and W. T. Vetterling, *Numerical Recipes in C: the Art of Scientific Computing* (Cambridge University, New York, 1988).
14. M. Abramowitz and I. A. Stegun, *Handbook of Mathematical Functions* (Dover, New York, 1965), p. 360, formula 9.1.8.
15. R. Barakat, "Application of the sampling theorem to optical diffraction theory," J. Opt. Soc. Am. **54**, 921–930 (1964).
16. D. R. Williams and N. J. Coletta, "Cone spacing and the visual resolution limit," J. Opt. Soc. Am. A **4**, 1514–1523 (1987).
17. J. W. Goodman, *Introduction to Fourier Optics*, 2nd ed. (McGraw-Hill, New York, 1996), Chap. 2, Sec. 2.4.
18. V. Lakshminarayanan and J. M. Enoch, "Biological Waveguides" in *Handbook of Optics Vol. III*, 2nd ed., M. Bass, ed. (McGraw-Hill, New York, 2001), Chap. 9.
19. R. Dändliker, "Rotational effects of polarization in optical fibers," in *Anisotropic and Non-Linear Optical Waveguides*, C. G. Someda and G. Stegman, eds. (Elsevier, Amsterdam, 1992), p. 42, Sec. 2.2.
20. L. D. Landau and E. M. Lifshitz, *Electrodynamics of Continuous Media* (Pergamon, Oxford, 1960), Chap. XI, Sec. 81.
21. S. Choi, M. Kono, and J. M. Enoch, "Evidence for Transient Strains at the Optics Disc and Nerve in Myopia: I. Stiles-Crawford Effect Studies Performed Over Time," presented at the Annual Meeting of Association for Research in Vision and Ophthalmology, Fort Lauderdale, Florida, May 5–10, 2002.
22. J. Limeres, M. L. Calvo, V. Lakshminarayanan, and J. M. Enoch, "Stress sensor based on light scattering by an array of birefringent optical waveguides," in *International Commission for Optics XIX: Optics for the Quality of Life*, A. Consortini and G. C. Righini, eds., Proc. SPIE **4829**, 881–882 (2002).